American Mineralogist, Volume 74, pages 466–475, 1989

Estimated solubility products and fields of stability for cryptomelane, nsutite, birnessite, and lithiophorite based on natural lateritic weathering sequences

Sylvie Parc, Daniel Nahon

Laboratorie de Géologie Dynamique et de Pétrologie de la Surface, CNRS, U.A. 132, Faculté de Saint-Jérôme, 13397 Marseille Cedex 13, France

Yves Tardy

Institut de Géologie, Centre CNRS de Sédimentologie et de Géochimie de la Surface, 1 rue Blessig, 67084 Strasbourg Cedex, France

Philippe Vieillard

Laboratoire de Pétrologie de la Surface, CNRS, U.A. 721, Université de Poitiers, 40 avenue du Recteur Pineau, 86022 Poitiers Cedex, France

Abstract

In Mn weathering profiles, the poorly crystallized minerals birnessite, cryptomelane, nsutite, and lithiophorite are the major manganese oxides. New stability fields for these minerals are proposed, based upon parageneses observed in natural conditions and upon the composition and oxidation state of Mn obtained from recent crystal-structure refinements of these minerals. The two major sequences revealed by Mn lateritic weathering profiles in Africa and Brazil are the following:

rhodochrosite + illite → cryptomelane + kaolinite → nsutite + kaolinite → lithiophorite → gibbsite

manganese silicates → birnessite + kaolinite → nsutite + kaolinite → pyrolusite + kaolinite → kaolinite → gibbsite.

Gibbs free energies of Mn-bearing minerals that are formed during weathering were estimated so as to fit the observed parageneses in natural weathering profiles.

Introduction

Lateritic weathering profiles either of Mn^{2+}-bearing carbonates in sedimentary parent rocks at Moanda (Gabon) and at Azul (Brazil) or of Mn^{2+}-bearing silicates at Ziemougoula (Ivory Coast) contain various Mn^{3+} and Mn^{4+} oxides and hydroxides. Among these major manganese oxy-hydroxides, manganite ($Mn^{3+}OOH$) and pyrolusite ($Mn^{4+}O_2$) are well crystallized. But cryptomelane ($K_xMn^{4+}_{8-x}Mn^{3+}_xO_{16}$), nsutite ($Mn^{4+}_{1-y}Mn^{3+}_yO_{2-y}(OH)_y$), birnessite ($Mn^{4+}_5Mn^{3+}_2O_{13}\cdot 5H_2O$), and lithiophorite ($Al_2$-$Mn^{4+}_3O_9\cdot 3H_2O$) are often poorly crystallized. The chemistry and structure of the last four minerals have been worked out by Potter and Rossman (1979), Pauling and Kamb (1982), Post et al. (1982), Turner and Buseck (1983), Hypolito et al. (1984), Giovanoli (1985), Vicat et al. (1986), and Manceau et al. (1987). The Gibbs free energies of formation of these minerals are either unknown (for lithiophorite) or unreliable because of the lack of good crystallochemical refinements for birnessite, cryptomelane, and nsutite at the time when ΔG_f^0 values were calculated (e.g., Bricker, 1965), or as shown herein inconsistent with parageneses observed in the lateritic profiles mentioned above (for nsutite and cryptomelane).

The purpose of this study is to estimate ΔG_f^0 values for nsutite, cryptomelane, birnessite, and lithiophorite that are consistent with petrographic and mineralogical observations of Mn lateritic weathering profiles, summarized in the first part of this paper. Although weathering is of course a disequilibrium process in an overall sense, we assume here that it proceeds by partial and local equilibrium steps. This assumption is justified by common evidence (summarized by Aagaard and Helgeson, 1983, Fig. 13) that many minerals formed during weathering are in equilibrium with their associated interstitial waters.

Parageneses of lateritic weathering of Mn-bearing parent rocks

Lateritic profiles developed on manganiferous metamorphic rocks in the Ziemougoula area (northwest Ivory Coast), on manganiferous sedimentary rocks in the Moanda area (Gabon), and in the Azul area (northern Brazil) are good examples for observing complete evolutions from Mn^{2+}-bearing parent minerals to Mn^{4+} oxides.

At Ziemougoula (Nahon et al., 1984, 1985), the weathering profile is about 25 m thick and has developed on a Birrimian metamorphic parent rock consisting roughly of 50% tephroite, 35% spessartine garnet, 7.5% quartz, 5% manganoan calcite, 2% Mn-rich chlorite and 0.5% sulfides. The observed profile is sketched in Figure 1, which shows the different responses of the initial minerals to weathering. The order of stability of the Mn parent min-

0003–004X/89/0304–0466$02.00

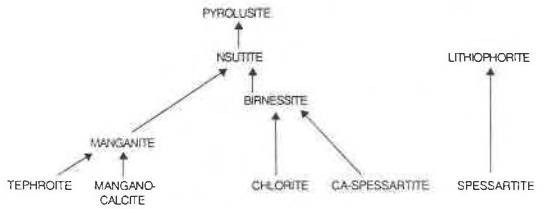

Fig. 1. Mineral sequences observed in the lateritic profile of Ziemougoula (Ivory Coast).

erals is tephroite < manganoan calcite < Mn-rich chlorite < Mn-bearing garnet. Consequently, tephroite occurs only at the base of the profile, while the more stable minerals persist higher in the profile. The rate of alteration of garnets differs depending on their chemical composition; the Ca-bearing spessartine alters first and weathers more rapidly than the Ca-free garnet. At the extreme base of the profile, only manganite ($Mn^{3+}OOH$) develops from tephroite and manganoan calcite weathering, while other parent minerals remain unweathered. At the top of the profile, nsutite + pyrolusite + lithiophorite occur and form together within the same horizon. Lithiophorite replaces spessartine late in the weathering process. Nsutite replaces either earlier-formed manganite or birnessite, which occurs in the middle of the profile and which itself replaces chlorite and Ca-bearing spessartine. Small amounts of pyrolusite result from the alteration of nsutite.

The second profile occurs at the Moanda weathering ore-body, in Gabon. The Precambrian sedimentary parent rock is a black calcareous shale consisting of 56% rhodochrosite, 23% illite, 11% detrital silt-sized quartz, 4% pyrite, and 6% organic matter. A general weathering profile has developed (Perseil and Bouladon, 1971; Weber et al., 1979; Nahon et al., 1983) and consists of manganite + pyrolusite bands nearest the fresh rock and cryptomelane, nsutite, a second generation of pyrolusite, and lithiophorite higher up, with in some places, a direct transition from rhodochrosite to cryptomelane.

The third example is that of Azul area near Carajas (northern Brazil). The Precambrian parent rock is a black silty shale consisting of 30 to 65% rhodochrosite, 15 to 30% quartz, 15 to 25% detrital muscovite and authigenetic kaolinite, 0 to 10% detrital feldspar, 5% pyrite, and organic matter. Valarelli et al. (1978) and Bernardelli and Beisiegel (1978) have shown that weathering of this rhodochrosite-bearing unit leads to thick oxidized horizons. In the lower part of the oxidized zone the sequence is cryptomelane nearest the fresh rock, followed upward by nsutite, pyrolusite, a second generation of cryptomelane, and then lithiophorite (Beauvais et al., 1987).

Very similar profiles have been described in other examples in Brazil (Horen, 1953; Bittencourt, 1973), and in Africa (Sorem and Cameron, 1960; Perseil and Grandin, 1978; Boeglin, 1981). The generalized profile always shows oxides with low Mn oxidation number near the bottom and high Mn oxidation number ones toward the

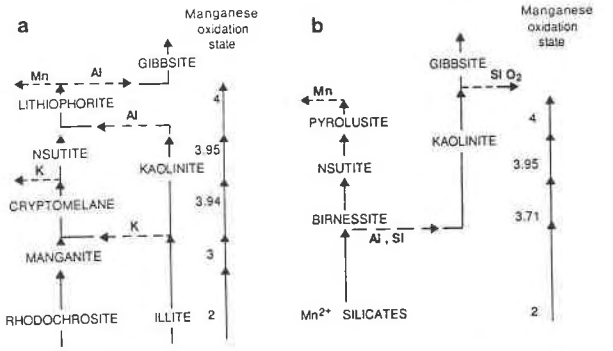

Fig. 2. Two different sequences of weathering parageneses of manganese protores (each Mn weathering stage is characterized by the average or real oxidation state of Mn). Minerals are formed by replacement in the order shown; each arrow point marks the first appearance of the replacing mineral in the profile. Dashed lines with arrows indicate where ions are released to the pore fluid.

surface (Fig. 2a). But there are minor "inversions" of oxidation numbers because of other components. For example, K^+ ions released from illite alteration into kaolinite in the middle of the profile promote formation of cryptomelane (Fig. 2b). High in the profile, Al^{3+} ions released by later dissolution of kaolinite can promote formation of lithiophorite (Fig. 2b) in the presence of Mn^{2+} ions. The parent rock's composition and mineral assemblage thus control which manganese oxides can eventually form. These "retrogressive" stages are commonly found in the weathering profiles and can explain the occurrence of several generations of cryptomelanes and lithiophorites. This is illustrated by Figures 3 and 4, which respectively show the progressive replacement of pyrolusite by cryptomelane and by lithiophorite, in the weathering profile of Moanda.

Thermodynamic approach of the stability of different Mn minerals

Previous work

Studies of aqueous Mn species in natural solutions (Hem, 1963; Bricker, 1965; Lind et al., 1987) have shown that within the stability field of water, Mn^{2+} is the major ion in solution. Therefore, all the Eh-pH diagrams pre-

Table 1. Gibbs free energies of formation of Mn minerals and different ions involved in the system MnO_2-Al_2O_3-SiO_2-H_2O at 25 °C and 1 atm

Ions and minerals	ΔG^0 (kJ·mol^{-1})	References
Mn^{2+}	−228.0	Robie et al. (1978)
Al^{3+}	−489.40	Robie et al. (1978)
K^+	−282.48	CODATA (1977)
H_4SiO_4	−1308.0	Robie et al. (1978)
H_2O	−237.19	CODATA (1977)
β-MnO_2	−465.14	Bricker (1965)
γ-MnOOH	−557.73	Bricker (1965)
$MnCO_3$	−816.07	Helgeson et al. (1978)

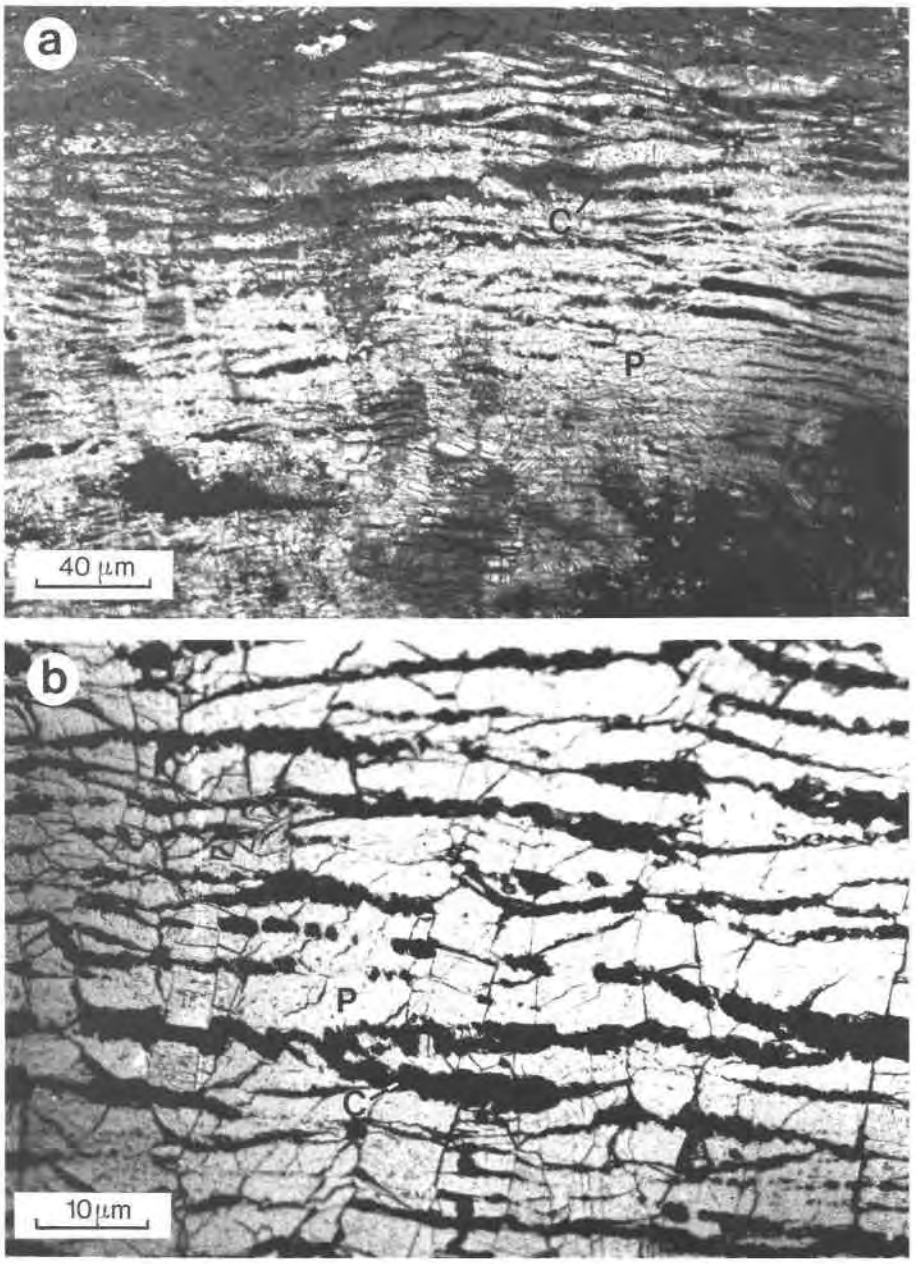

Fig. 3. (**a**) Retrogressive replacement of pyrolusite into cryptomelane, observed under reflected light. P is pyrolusite; C is cryptomelane (in gray). (**b**) Detail of (a): vertical columnar crystals of pyrolusite replaced by subhorizontal layers of cryptomelane.

sented in the literature have been established by using Mn^{2+} as the conventional ion present in solution. Table 1 lists the Gibbs free energies of formation for Mn ions and minerals and other aqueous species involved in this work.

Relations between stability fields for Mn minerals with different oxidation states such as rhodochrosite ($Mn^{2+}CO_3$), manganite ($Mn^{3+}OOH$), and pyrolusite ($Mn^{4+}O_2$) have already been established in Eh-pH diagrams (Fig. 36 in Bricker, 1965). They can also be written as a function of f_{O_2}, the oxygen fugacity (Garrels and Christ, 1965). However, in representing stability fields of birnessite, nsutite, and cryptomelane, earlier workers used the then-accepted but inaccurate formulae for these significant minerals. In this study, we take account of recent crystal-structure determinations that produce better estimates of the oxidation states of Mn in the minerals and their compositions.

Recent publications give refinements for cryptomelane, nsutite, and birnessite. The cryptomelane structure consists of a framework of double chains of edge-sharing Mn-O octahedra containing large tunnels filled with K^+

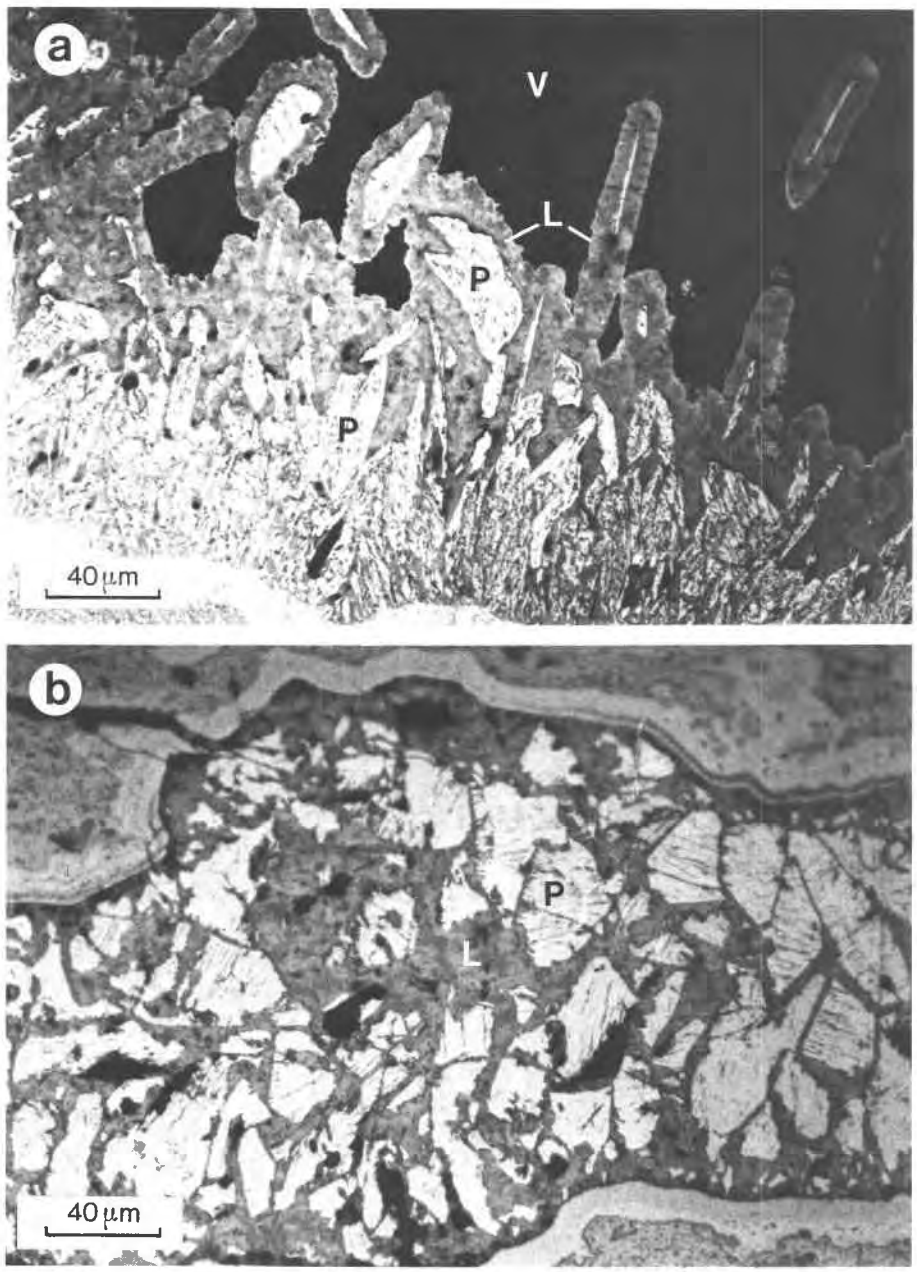

Fig. 4. (**a**) Retrogressive replacement of pyrolusite into lithiophorite, observed under reflected light. P is pyrolusite, L is lithiophorite, V is void. (**b**) Columnar crystals of pyrolusite that are cut into several fragments by lithiophorite. Each fragment keeps its original crystallographical orientation, which shows an in situ replacement of pyrolusite by lithiophorite.

ions. Most of the manganese is Mn^{4+}, but some Mn^{3+} substitutes for Mn^{4+} to balance the positive charge of tunnel cations (Post et al., 1982; Hypolito et al., 1984). The chemical formula can be written as $K_xMn^{4+}_{8-x}Mn^{3+}_xO_{16}$ (Vicat et al., 1986) with x ranging from 0.2 to 1.0 in cryptomelanes from lateritic profiles. Microprobe analyses of cryptomelanes from Azul (Brazil) and from Moanda (Gabon) give the average formulae $K_{0.5}Mn^{4+}_{7.5}Mn^{3+}_{0.5}O_{16}$ and $K_{0.6}Mn^{4+}_{7.4}Mn^{3+}_{0.6}O_{16}$ (Beauvais, 1984).

The formula proposed for nsutite by Giovanoli and Leuenberger (1969) and chosen here is $Mn^{4+}_{1-y}Mn^{3+}_yO_{2-y}(OH)_y$. Because nsutite consistently replaces cryptomelane in the profile at Moanda, we believe it is reasonable to assume that nsutite is more oxidized (i.e., contains less Mn^{3+}) than cryptomelane, a condition that requires that $y < 0.6/8 = 0.075$ (0.05, for example), where as we have seen, 0.6 is the extent of substitution of Mn^{3+} for Mn^{4+} in the formula of cryptomelane containing 8

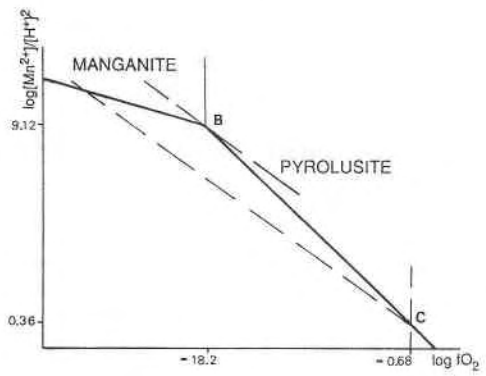

Fig. 5. Sketch of limits of stability fields (dashed lines lying through *B* and *C*) for manganese oxides observed in natural profiles with Mn oxidation states ranging from 3+ to 4+.

Mn atoms. The degree of substitution for y can reach 0.09 for nsutites from Ghana, Greece, and Mexico (Table 1, in Zwicker et al., 1962).

The structure of birnessite has been studied by Giovanoli (1980) and Giovanoli et al. (1970, 1971). Birnessite is composed of two types of layers; layers of Mn-O octahedra alternate with layers of hydroxyl and water. Its chemical composition is $Mn_5^{4+}Mn_2^{3+}O_{13}\cdot 5H_2O$.

Gibbs free-energy estimates

We now estimate the Gibbs free energies of formation of nsutite, cryptomelane, birnessite, and lithiophorite ($Al_2Mn_3^{4+}O_9\cdot 3H_2O$). As a guide, we use as chemical compositions for these minerals those from the manganese deposits of Moanda (Gabon), Ziemougoula (Ivory Coast), and Azul (Brazil) because parageneses and chemical compositions have been carefully worked out at those localities. The ΔG_f^0 values are estimated in such a way that the mineral stability fields constructed with them are compatible with the sequence of replacements observed microscopically in weathering profiles. In all the following calculations, the activity of water is assumed to be unity.

By using the thermodynamic data proposed in Table 1, one obtains an equilibrium oxygen fugacity of $10^{-18.2}$ atm that separates the stability field of manganite from the one of pyrolusite. The equilibria between these minerals and an aqueous solution are

$$Mn^{3+}OOH_{(man)} + 2H^+_{(aq)} = Mn^{2+}_{(aq)} + 1.5H_2O_{(aq)} + 0.25O_{2(g)} \quad (1)$$

$$Mn^{4+}O_{2(pyr)} + 2H^+_{(aq)} = Mn^{2+}_{(aq)} + H_2O + 0.5O_{2(g)}. \quad (2)$$

In a diagram of $\log[Mn^{2+}]/[H^+]^2$ vs. $\log f_{O_2}$, the straight lines separating these minerals stability fields from solutions intersect at this equilibrium fugacity of $10^{-18.2}$ and the corresponding $\log[Mn^{2+}]/[H^+]^2 = 9.12$.

Consequently, in the same kind of diagram, the lines for nsutite, cryptomelane, and birnessite, which all show intermediate degrees of Mn oxidation, must appear between the two points B and C, the coordinates ($\log f_{O_2}$, $\log[Mn^{2+}]/[H^+]^2$) of which are, respectively, (−18.2, 9.12) and (−0.68, 0.36) where −0.68 represents the log of p_{O_2} in air (Fig. 5).

Estimation of ΔG_f^0 of nsutite. The equilibrium between nsutite and aqueous solution can be represented by

$$Mn^{4+}_{1-y}Mn^{3+}_yO_{2-y}(OH)_{y(nsu)} + 2H^+_{(aq)} = Mn^{2+}_{(aq)} + (1 + y/2)H_2O_{(l)} + [(2 - y)/4]O_{2(g)}. \quad (3)$$

In Equation 3, y stands for the amount of Mn^{3+} substituting for Mn^{4+}, and the corresponding log K at equilibrium is given in Table 2. On a $\log[Mn^{2+}]/[H^+]^2$ vs. $\log f_{O_2}$ diagram, manganite and pyrolusite slopes are respectively −0.25 and −0.5. The slope of the nsutite equilibrium line is $-(2 - y)/4$, intermediate between −0.25 and −0.5. All of them are shown in the sketch of Figure 5. For nsutite to appear, as it in fact does in lateritic profiles, and for it to have a field between those for manganite and pyrolusite, its line must lie somewhere between point *B* (intersection of manganite and pyrolusite lines) and point *C*, which is fixed by the condition that nsutite cannot occur for $f_{O_2} > f^{air}_{O_2}$ because pyrolusite is more stable. Thus log K_{nsu} for point *B* is $\log K_{nsu} = 0.02 + 4.55y$ and for point C is $\log K_{nsu} = 0.02 + 0.17y$. Consequently, for $y = 0.05$, the log K for $Mn^{4+}_{0.95}Mn^{3+}_{0.05}O_{1.95}(OH)_{0.05}$ has to be between 0.03 and 0.25. In this case, the uncertainty on the ΔG_f^0 back-calculated from Equation 3 is less than 1.5 kJ (Table 3). For the most Mn^{3+}-rich nsutites described in the literature, for which the value of y is 0.09, the uncertainty on ΔG_f^0 is still small. Thus the ΔG_f^0 of nsutite turns out to be very closely bracketed by the condition that the mineral does form in lateritic profiles, regardless of the value of y.

Estimation of ΔG_f^0 for birnessite and cryptomelane. The same method has been applied for the estimation of ΔG_f^0 for birnessite and cryptomelane.

The equilibrium between cryptomelane and aqueous solution is

$$K_xMn^{4+}_{8-x}Mn^{3+}_xO_{16(cry)} + (16 + x)H^+_{(aq)} = xK^+_{(aq)} + 8Mn^{2+}_{(aq)} + (8 + x/2)H_2O_{(l)} + (4 - x/4)O_{2(g)}. \quad (4)$$

The solubility product at 25 °C for cryptomelane is listed in Table 2. It has been calculated assuming $\log[K^+]/[H^+] = 3$, which corresponds to the equilibrium illite-kaolinite at 25 °C and 1 atm (Aagaard and Helgeson, 1983). This value is in agreement with the observations in the first stage of the lateritic manganese ore at Moanda (Fig. 2b). As mentioned above, as kaolinite replaces illite (the K-bearing mineral in the parent rock) K^+ ions are leached into solution (i.e., $\log[K^+]/[H^+]$ increases), which promotes crystallization of cryptomelane. Furthermore as cryptomelane forms, assuming a constant value for pH, a drop in $\log[K^+]/[H^+]$ can be observed, and then nsutite appears as the most stable phase, replacing cryptomelane. The deduced log K estimates for different cryptomelanes are shown in Table 3. These estimates are well bracketed for cryptomelanes that have a small degree of substitution of Mn^{3+} for Mn^{4+} whereas the range of values of ΔG_f^0 becomes larger for high-K cryptomelanes. These ranges

TABLE 2. Chemical formulae and solubility products of the principal minerals involved in the weathering of Mn-bearing rocks

Mineral name and chemical formula	Solubility products at 25 °C (for $a_{H_2O} = 1$)	References
Pyrolusite		
$Mn^{4+}O_2$	$\log[Mn^{2+}]/[H^+]^2 + 0.5 \log f_{O_2} = 0.02$	Bricker (1965)
Lithiophorite		
$Al_2Mn^{4+}O_9 \cdot 3H_2O$	$3 \log[Mn^{2+}]/[H^+]^2 + 2 \log[Al^{3+}]/[H^+]^3 + \frac{3}{2}\log f_{O_2} = 15.5$	This paper
Nsutite		
$Mn^{4+}_{1-y}Mn^{3+}_yO_{2-y}(OH)_y$	$\log[Mn^{2+}]/[H^+]^2 + [(2 - y)/4]\log f_{O_2} = 0.02 + 0.17y^*$ $= 0.02 + 4.55y\dagger$	This paper
Cryptomelane		
$K_xMn^{4+}_{8-x}Mn^{3+}_xO_{16}$	$8 \log[Mn^{2+}]/[H^+]^2 + x \log[K^+]/[H^+] + (4 - x/4)\log f_{O_2} = 0.16 + 3.17x^*$ $= 0.16 + 7.55x\dagger$	This paper
Birnessite		
$Mn^{4+}_5Mn^{3+}_2O_{13} \cdot 5H_2O$	$7 \log[Mn^{2+}]/[H^+]^2 + 3 \log f_{O_2} = 0.48^*$ $= 9.24\dagger$	This paper
Manganite		
$Mn^{3+}OOH$	$\log[Mn^{2+}]/[H^+]^2 + 0.25 \log f_{O_2} = 4.57$	Bricker (1965)
Rhodochrosite		
$Mn^{2+}CO_3$	$\log[Mn^{2+}]/[H^+]^2 + \log f_{CO_2} = 7.62$	Helgeson et al. (1978)
Gibbsite		
$Al(OH)_3$	$\log[Al^{3+}]/[H^+]^3 = 8.205$	Fritz and Tardy (1973)
Kaolinite		
$Al_2Si_2O_5(OH)_4$	$2 \log[Al^{3+}]/[H^+]^3 + 2 \log[H_4SiO_4] = 7.41$	Fritz and Tardy (1973)

* and † Values of log K determined for the largest and the smallest stability fields in Fig. 5, respectively.

of values also differ from one composition to another, which clearly points out that appropriate formulae have to be taken into account to establish stability relationships between different manganese oxides.

If there is no K^+ in the system, as at Ziemougoula, then birnessite instead of cryptomelane can become the intermediate phase between manganite and nsutite. Its solubility equilibrium is

$$Mn^{4+}_5Mn^{3+}_2O_{13} \cdot 5H_2O_{(bir)} + 14H^+_{(aq)} = 7Mn^{2+}_{(aq)} + 12H_2O_{(l)} + 3O_{2(aq)}. \quad (5)$$

The ranges of values for its solubility product correspond to the extreme positions for which the line for birnessite lies between points B and C (Fig. 5). In this case, the uncertainty on ΔG^0_f of birnessite is quite large. However, birnessite could be better bracketed if the exact value of ΔG^0_f was known because birnessite always alters to nsutite but not directly to pyrolusite. The relative stability fields for manganite, birnessite, and nsutite are shown in a $\log[Mn^{2+}]/[H^+]^2$ vs. $\log f_{O_2}$ diagram for indicated values of log K for nsutite and birnessite in Figure 6. A similar diagram has been drawn for cryptomelane in Figure 7. In both of these diagrams, rhodochrosite has been introduced in the system in order to show the influence of the CO_2 partial pressure. The $MnCO_3$ solubility equilibrium is

$$Mn^{2+}CO_{3(rho)} + 2H^+_{(aq)} = Mn^{2+}_{(aq)} + CO_{2(g)} + H_2O_{(l)}. \quad (6)$$

For high CO_2 pressures ($\log f_{CO_2} > -2.0$) it seems that manganite is not stable and that birnessite, or cryptomelane (if there are enough K^+ ions available in solution), can develop directly from the weathering of manganese carbonates. Rhodochrosite can also alter to cryptomelane for lower CO_2 partial pressures if large amounts of K^+ ions are available in the system (i.e., $\log[K^+]/[H^+] > 3$,

TABLE 3.—Ranges of values for log K and ΔG^0_f

Mineral	Log K at 25 °C, 1 atm ($a_{H_2O} = 1$)	ΔG^0_f (kJ·mol^{-1})
$Mn^{4+}_{0.95}Mn^{3+}_{0.05}O_{1.95}(OH)_{0.05}$ (nsutite)	0.03 to 0.25	−469.7 to −471.0
$Mn^{4+}_{0.91}Mn^{3+}_{0.09}O_{1.91}(OH)_{0.09}$ (nsutite)	0.04 to 0.43	−468.7 to −471.1
$K_{0.2}Mn^{4+}_{7.8}Mn^{3+}_{0.2}O_{16}$ (cryptomelane)	0.24 to 0.79	−3800.4 to −3797.2
$K_{0.5}Mn^{4+}_{7.5}Mn^{3+}_{0.5}O_{16}$ (cryptomelane)	1.75 to 3.93	−3912.1 to −3899.6
$KMn^{4+}Mn^{3+}O_{16}$ (cryptomelane)	3.17 to 7.55	−4104.5 to −4079.5
$Mn^{4+}_5Mn^{3+}_2O_{13} \cdot 5H_2O$ (birnessite)	0.48 to 9.24	−4439.5 to −4389.5

Note: The ranges given for the various chemical compositions of nsutites, cryptomelanes, and birnessite are consistent with those obtained for such minerals from lateritic profiles. For each mineral, the first and the second values of log K and ΔG^0_f are given for the largest and the smallest stability fields, in Figure 5, respectively.

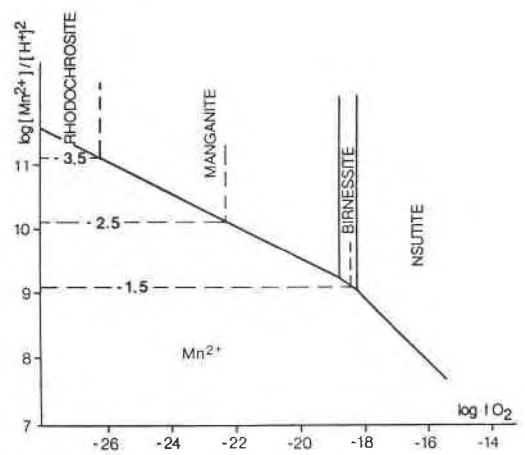

Fig. 6. Stability fields of nsutite ($Mn^{4+}_{0.95}Mn^{3+}_{0.05}O_{1.95}(OH)_{0.05}$) and birnessite ($Mn^{4+}_5Mn^{3+}_2O_{13} \cdot 5H_2O$) at 25 °C and 1 atm (for log $K_{nsu} = 0.68$ and for log $K_{bir} = 8.63$). The tie-lines represent the different limits of the rhodochrosite stability field as a function of $\log f_{CO_2}$.

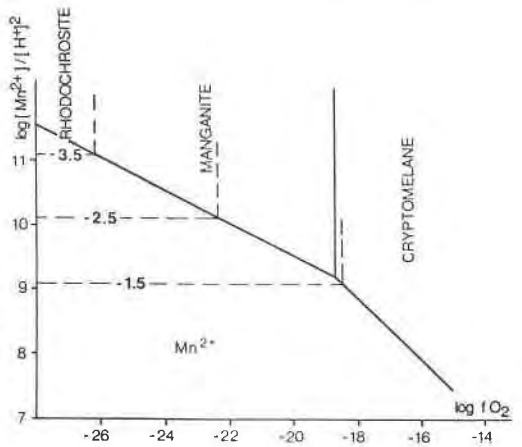

Fig. 7. Stability field of cryptomelane ($K_{0.5}Mn^{4+}_{7.5}Mn^{3+}_{0.5}O_{16}$) at 25 °C and 1 atm, for log K_{cry} = 3.23 and for log[K^+]/[H^+] = 3. The tie-lines represent the different limits of the rhodochrosite stability field as a function of log f_{CO_2}.

for example). Such replacements are observed in manganese lateritic profiles (Table XXI in Roy, 1981).

The stability of lithiophorite. No thermodynamic data were found in the literature for lithiophorite. This mineral has been studied apart from the other manganese oxides because it contains both Mn and Al. The chemical formula proposed by de Villiers and van der Walt in 1945, $LiAl_2Mn_3O_9 \cdot 3H_2O$, is in accordance with the structure in which layers of MnO_6 and $(Al,Li)(OH)_6$ octahedra alternate along the *c* axis (Wadsley, 1952). But, at Ziemougoula (Ivory Coast) or at Moanda (Gabon), as well as in many other manganese deposits, the quantity of Li in lithiophorite is very small. Therefore, the following chemical formula of lithiophorite will be used for further calculations: $Al_2Mn_3O_9 \cdot 3H_2O$.

In the lateritic profile at Moanda (Gabon), lithiophorite replaces pyrolusite (Fig. 2b) as well as nsutite at the top of the platy horizon, in zones where relicts of kaolinite are still present. Locally, crystals of gibbsite seem to develop from lithiophorite (Beauvais, 1984). Thus, this mineral appears as an intermediate phase between manganese oxides (pyrolusite, nsutite) and aluminum hydroxide (gibbsite). The corresponding solution and mineral equilibria are the following:

$$Al(OH)_{3(gib)} + 3H^+_{(aq)} = Al^{3+}_{(aq)} + 3H_2O_{(l)} \quad (7)$$

$$Al_2Si_2O_5(OH)_{4(kao)} + 6H^+_{(aq)} = 2Al^{3+}_{(aq)} + 2(H_4SiO_4)^0_{(aq)} + H_2O_{(l)} \quad (8)$$

$$Al_2Mn^{4+}_3O_9 \cdot 3H_2O_{(lit)} + 12H^+_{(aq)} = 2Al^{3+}_{(aq)} + 3Mn^{2+}_{(aq)} + 9H_2O_{(l)} + 1.5O_{2(g)}. \quad (9)$$

The corresponding solubility products are given in Table 2.

Lithiophorite is formed by Mn^{4+} and Al^{3+} ions directly released from, respectively, pyrolusite and kaolinite still

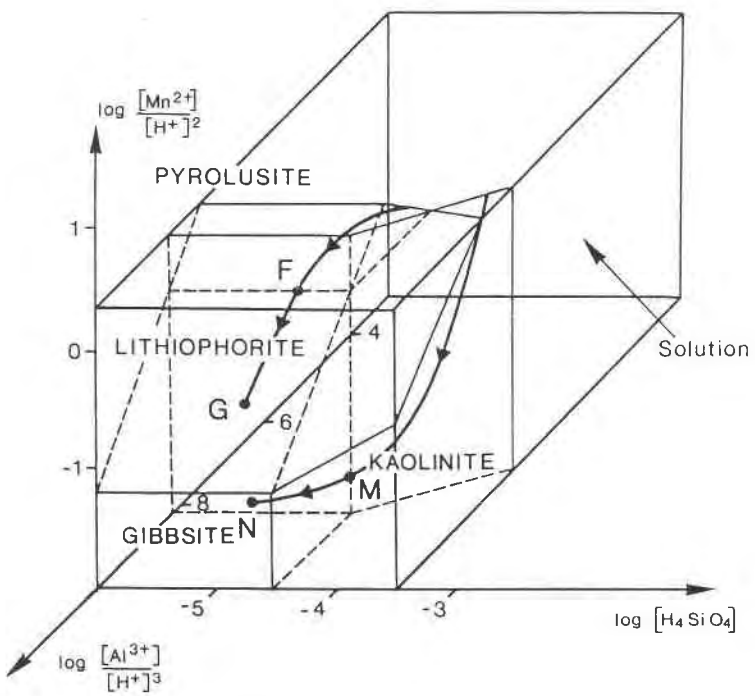

Fig. 8. Three-dimensional stability-field diagram (log[Mn^{2+}]/[H^+]^2 vs. log[H_4SiO_4] and log[Al^{3+}]/[H^+]^3) for pyrolusite, lithiophorite, gibbsite, and kaolinite at 25 °C and log f_{O_2} = −0.68, using the following solubility products: log K_{py} = 0.02, for pyrolusite; log K_{li} = 15.5, for lithiophorite; log k_{gi} = 8.205, for gibbsite; log K_{ka} = 7.41, for kaolinite. The arrows show two different pathways that represent common chemical evolution of natural solution.

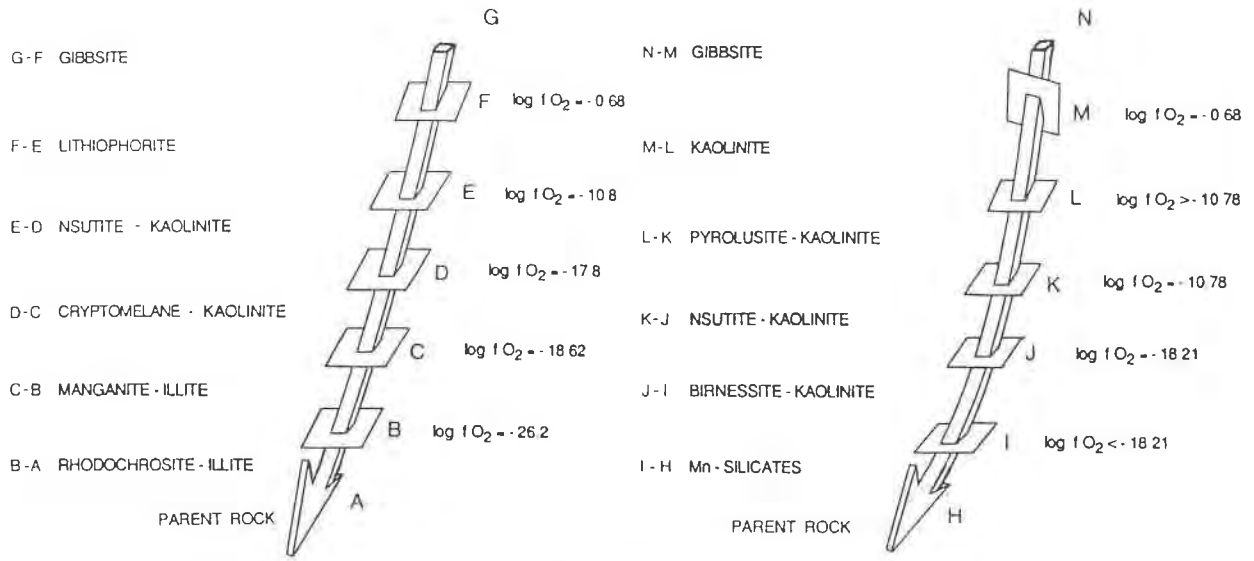

Fig. 9. Schematic chemical path of solutions during weathering of two Mn-bearing rocks. The arrow indicates the sense of circulation of the weathering solution.

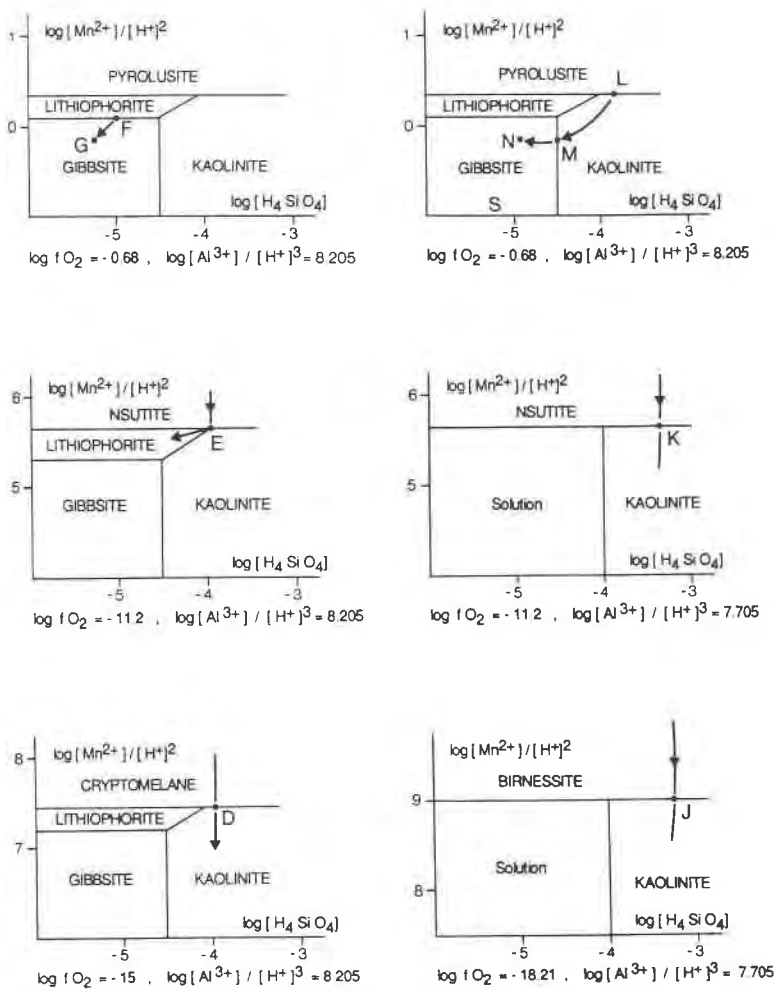

Fig. 10. Two-dimensional activity diagrams ($\log[Mn^{2+}]/[H^+]^2$, $\log[H_4SiO_4]$) for different values of $\log f_{O_2}$ and of $\log[Al^{3+}]/[H^+]^3$.

present in the system. Consequently, the Gibbs free energy of formation of lithiophorite can be estimated from the equilibrium reaction

$$3MnO_{2(pyr)} + Al_2Si_2O_5(OH)_{4(kao)} + 5H_2O_{(l)} = Al_2Mn_3O_9 \cdot 3H_2O_{(lit)} + 2H_4SiO_{4(aq)}. \quad (10)$$

$$\log K_r = 2 \log[H_4SiO_4]$$
$$\Delta G_f^0 (\text{lit}) = -2\Delta G_f^0(H_4SiO_4) + \Delta G_f^0(\text{kao}) + 3\Delta G_r^0(\text{pyr}) + 5\Delta G_f^0 (H_2O) + \Delta G_r^0.$$

The range of values of $\log[H_4SiO_4]$ is limited to the boundaries of the stability field of kaolinite at 25 °C and 1 atm, i.e., the interval −4.5 to −3.5, the former corresponding to the gibbsite-kaolinite equilibrium (Fritz and Tardy, 1973), the latter to the kaolinite-illite equilibrium (Aagaard and Helgeson, 1983). The calculated Gibbs free energy of formation of lithiophorite is then

$$\Delta G_f^0(\text{lit}) = -3709.8 + 5.71 \text{ kJ} \cdot \text{mol}^{-1}.$$

The stability field of lithiophorite relative to those of pyrolusite, kaolinite, and gibbsite is represented in a three-dimensional diagram: $\log[Mn^{2+}]/[H^+]^2$, $\log[Al^{3+}]/[H^+]^3$, and $\log[H_4SiO_4]$ for $\log f_{O_2} = -0.68$ and for $\Delta G_f^0(\text{lit}) = -3709.8$ kJ·mol^{-1} (Fig. 8).

This block diagram shows that $\log[Al^{3+}]/[H^+]^3$ plays a prominent part in governing the crystallization of minerals. For a value of 8.205, gibbsite is stable. Below 8.205, there are two possibilities: (1) For $\log[H_4SiO_4]$ higher than −4.5, kaolinite is in equilibrium with the solution. (2) If there are enough Mn ions in solution, lithiophorite is formed. Its stability field is limited to the range $7.7 < \log[Al^{3+}]/[H^+]^3 < 8.205$ for $f_{O_2} = 10^{-0.68}$ (oxygen partial pressure in the air). Calculations based upon the solubility products given in Table 2 show that for lower values of $\log f_{O_2}$, this field becomes narrower and disappears for reducing environments (and, for example, for $\log f_{O_2} < -19.5$).

Two simulated chemical weathering paths from *A* to *G* and from *H* to *N*, corresponding to the sequences of Figure 2b, are presented in Figure 9. Details are given in the two-dimensional diagrams of Figure 10 for the last weathering stages and for different values of $\log f_{O_2}$. In slightly oxidizing environments, parageneses such as cryptomelane-kaolinite and birnessite-kaolinite are explained thermodynamically. And as the environment becomes more oxidizing, that is to say, in the upper horizons, these parageneses are replaced by nsutite-kaolinite, then pyrolusite-kaolinite or lithiophorite, depending on the initial composition of the bedrock.

Conclusion

We have estimated the ΔG_f^0 values of nsutite, cryptomelane, birnessite, and lithiophorite taking account of recent refinements of the structure and the chemical composition of these oxides and imposing the condition that these minerals have stability fields arranged in the same sequence as the minerals themselves occur in well-studied lateritic profiles.

Nsutite, cryptomelane, and birnessite have been compared to pyrolusite and manganite for which the ΔG_f^0 values were taken from Bricker (1965). This condition is actually very restrictive in the case of nsutites and even cryptomelanes but is weaker in the case of birnessite. In the stability diagrams depicted, the different sequences observed in Mn lateritic weathering profiles have been represented. Only pyrolusite is stable in pure and highly oxidizing environments. Next, nsutite appears in less oxidizing environments, followed by birnessite for even less oxidizing ones, whereas in the presence of cations (such as K^+, for example), other manganese oxides (cryptomelane in the present case) are generally formed.

To complete the study of Mn lateritic weathering profiles, the Gibbs free energy of formation of lithiophorite, for which no thermodynamic data were available, has been estimated. The final diagrams show that this (Mn,Al) oxi-hydroxide can appear as an intermediate phase between various manganese oxides and gibbsite, as it does in the Mn weathering profiles, especially in the upper horizons.

Such observations illustrate some geochemical interactions between ions and Mn species in lateritic weathering. Parameters such as the initial composition of the bedrocks (manganese carbonates or manganese silicates and minerals bearing other cations such as K^+ in illite) and partial pressure of CO_2 influence the initial crystallization either of manganite, birnessite, or cryptomelane.

References cited

Aagaard, P., and Helgeson, H.C. (1983) Activity/composition relations among silicates and aqueous solutions: II. Chemical and thermodynamic consequences of ideal mixing of atoms on homological sites in montmorillonites, illites, and mixed layer clay. Clays and Clay Minerals, 31, 207–217.

Beauvais, A. (1984) Concentrations manganésifères latéritiques. Etude pétrologique de 2 gîtes sur roches sédimentaires précambriennes. Gisements de Moanda (Gabon) et d'Azul (Brésil). Thèse 3e cycle, 156 p. Université de Poitiers, Poitiers, France.

Beauvais, A., Melfi, A., Nahon, D., and Trescases, J.J. (1987) Pétrologie du gisement latéritique manganésifère d'Azul (Brésil). Mineralium Deposita, 22, 124–134.

Bernadelli, A.L., and Beisiegel, V.R. (1978) Geologica economica da jazida de manganês do Azul. Anais do XXX^e Congresso Brasileiro Geologia, Receife, 4, 1431–1444.

Bittencourt, A.V.L. (1973) Contribuçao as estudo genético do minério de manganês de Conselheiro Lafaiete, Minas Gerais. Thèse Sciences, 81 p. Universidade de São Paulo, São Paulo, Brazil.

Boeglin, J.L. (1981) Minéralogie et géochimie des gisements de manganèse de Conselheiro Lafaiete au Brésil et de Moanda au Gabon. Thèse 3e Cycle, 155 p. Toulouse, France.

Bricker, O. (1965) Some stability relations in the system $Mn-O_2-H_2O$ at 25 °C and one atmosphere total pressure. American Mineralogist, 50, 1296–1354.

Codata. (1977) CODATA recommended key values for thermodynamics. Codata Bulletin 28, 17 p.

de Villiers, J.E., and van der Walt, C.F.J. (1945) Lithiophorite from the Postmasburg manganese deposits. American Mineralogist, 30, 629–634.

Fritz, B., and Tardy, Y. (1973) Etude thermodynamique du système gibbsite, quartz, kaolinite. Application à la genèse des podzols et des bauxites. Bulletin des Sciences Géologiques, 26, 339–367.

Garrels, R., and Christ, C. (1965) Solutions, minerals, and equilibria, 450 p. Freeman Cooper and Company, San Francisco.

Giovanoli, R. (1980) A review on structural data of electrolytical and

chemical MnO_2 (EMD and CMD). 2nd International Symposium on Manganese Dioxide by the Japanese Electrochemical Society, Tokyo.
——— (1985) Layer structures and tunnel structures in manganates. Chemical Erde, 44, 227–244.
Giovanoli, R., and Leuenberger, V. (1969) Uber die Oxidation von Manganoxihydroxide. Helvetica Chimica Acta, 52, 2333–2347.
Giovanoli, R., Stahli, E., and Feitknecht, W. (1970) Über Oxidhydroxide des vierwertigen Mangans mit schichtengitter. 1. Mitteilung. Natrium mangan (II, III) manganat (IV). Helvetica Chimica Acta, 53, 209–220.
Giovanoli, R., Feitknecht, W., and Fischer, F. (1971) Über Oxidhydroxide des vierwertigen Mangans mit Schichtengitter 3. Mitteilung: Reduktion von Mangans (III) manganat (IV) mit Zintalkohol. Helvetica Chimica Acta, 54, 1112–1124.
Helgeson, H.C., Delany, J.M., Nesbitt, H.W., and Bird, D.K. (1978) Summary and critique of the thermodynamic properties of rock-forming minerals. American Journal of Science, 278 A, 1–229.
Hem, J.D. (1963) Chemical equilibria and rates of manganese oxidation. U.S. Geological Survey Water Supply Paper 1667A, 1–64.
Horen, A. (1953) The manganese mineralization at the Merid mine, Minas Gerais, Brazil. Ph. D. thesis, 224 p. Harvard University, Cambridge, Massachusetts.
Hypolito, R., Valarelli, J.V., Giovanoli, R., and Netto, S.M. (1984) Gibbs free energy of formation of synthetic cryptomelane. Chimia, 38, 427–428.
Lind, C., Hem, J., and Roberson, C. (1987) Reaction products of manganese-bearing waters. In R.C. Averett and D.M. McKnight, Eds., Chemical quality of water and the hydrologic cycle, p. 272–301. Lewis Publishers, Chelsea, Michigan.
Manceau, A., Llorca, S., and Calas, G. (1987) Crystal chemistry of cobalt and nickel in lithiophorite and asbolane from New Caledonia. Geochimica et Cosmochimica Acta, 51, 105–114.
Nahon, D., Beauvais, A., Boeglin, J.L., Ducloux, J., and N'ziengui-Mapangou, P. (1983) Manganite formation in the first stage of the lateritic manganese ores in Africa. Chemical Geology, 40, 25–42.
Nahon, D., Beauvais, A., N'ziengui-Mapangou, P., and Ducloux, J. (1984) Chemical weathering of Mn-garnets under lateritic conditions in northwest Ivory Coast (West Africa). Chemical Geology, 45, 53–71.
Nahon, D., Beauvais, A., and Trescases, J.J. (1985) Manganese concentration through chemical weathering of metamorphic rocks under lateritic conditions. In J.I. Drever, Ed., The chemistry of weathering, p. 277–291. Reidel, Boston.
Pauling, L., and Kamb, B. (1982) The crystal structure of lithiophorite. American Mineralogist, 67, 817–821.
Perseil, E.A., and Bouladon, J. (1971) Microstructures des oxydes de manganèse à la base du gisement de Moanda (Gabon) et leur signification génétique. Comptes Rendus de l'Académie des Sciences de Paris, 273, 278–279.
Perseil, E.A., and Grandin, G. (1978) Evolution minéralogique du manganèse dans trois gisements d'Afrique occidentale: Mokta, Tambao, Nsuta. Mineralium Deposita, 3, 295–321.
Post, J.E., von Dreele, R.B., and Buseck, P.R. (1982) Symmetry and cation displacements in hollandites: Structure refinements of hollandite, cryptomelane, and priderite. Acta Crystallographica, B38, 1056–1065.
Potter, R.M., and Rossman, G.R. (1979) The tetravalent manganese oxides: Identification, hydratation, and structural relationships by infrared spectroscopy. American Mineralogist, 64, 1199–1218.
Robie, R.A., Hemingway, B.S., and Fisher, J.R. (1978) Thermodynamic properties of minerals and related substances at 298.15 K and 1 bar pressure and at higher temperatures. U.S. Geological Survey Bulletin 1452, 456 p.
Roy, S. (1981) Manganese deposits. 458 p. Academic Press, London.
Sorem, R.K., and Cameron, E.M. (1960) Manganese oxides and associated minerals of the Nsuta manganese deposits, Ghana West Africa. Economic Geology, 55, 278–310.
Turner, S., and Buseck, P.R. (1983) Defects in nsutite (γ- MnO_2) and dry all battery efficiency. Nature, 304, 143–146.
Valarelli, J.V., Bernardelli, A., and Beisiegel, W.R. (1978) Aspectos genéticos do minério de manganês do Azul. Anais do XXX^{o} Congresso Brasileiro de Geologia, Recife, 4, 1670–1679.
Vicat, J., Fanchon, E., Strobel, P., and Duc Tran Qui (1986) The structure of $K_{1.33}Mn_8O_{16}$ and cation ordering in Hollandite-type structures. Acta Crystallographica, B42, 162–167.
Wadsley, A.D. (1952) The structure of lithiophorite, (Al, Li)MnO_2 $(OH)_2$. Acta Crystallographica, 5, 676–680.
Weber, F., Leclerc, J., and Millot, G. (1979) Epigénies manganésifères successives dans le gisement de Moanda (Gabon). Bulletin de la Société des Sciences Geologiques, Strasbourg, 32, 6, 147–164.
Zwicker, W.K., Groeneveld Meijer, W.O.J., and Jaffe, H.W. (1962) Nsutite, a widespread manganese oxide mineral. American Mineralogist, 47, 246–266.

Manuscript received October 19, 1987
Manuscript accepted September 13, 1988